INSTITUTE OF PHYSICS PUBLISHING MEASUREMENT SCIENCE AND TECHNOLOGY

Meas. Sci. Technol. **17** (2006) 101–110 doi:10.1088/0957-0233/17/1/017

Attitude measurement by artificial vision

F Truchetet, O Aubreton, P Gorria and O Laligant

Le2i, UMR 5158 CNRS—Université de Bourgogne, 12 rue de la fonderie, 71200 Le Creusot, France

E-mail: f.truchetet@iutlecreusot.u-bourgogne.fr

Received 11 March 2005, in final form 13 September 2005
Published 5 December 2005
Online at stacks.iop.org/MST/17/101

Abstract
The recent development of light and low-cost airborne platforms (microlight, drones, kites, balloons, . . .) has led to the need for simple and low-cost devices allowing attitude measurement with respect to a reference horizon of the platform itself or of an embedded setting. A theoretical study of the conditions for measuring attitude angles from artificial vision is proposed and an original practical algorithm allowing these measurements to be performed in real time is described. An implementation in a CMOS retina circuit is also presented. These points are illustrated by experiments confirming the feasibility of the device.

Keywords: artificial vision, image processing, attitude measurement, airborne imaging

(Some figures in this article are in colour only in the electronic version)

1. Introduction

The recent development of light and low-cost airborne platforms (microlight aircraft, drones, kites, balloons, . . .) has introduced the need for simple and low-cost devices allowing the measurement of attitude with respect to a reference horizon of the platform itself or of an embedded setting. Only the gyro horizon is able to give autonomously inertial reference data whatever the external situation. There exist many commercial devices using the gyro horizon or a three-axis magnetometer, a piezoelectric vibration gyroscope (for angular velocity) and even a two-axis electrolytic clinometer; an example can be found in [11]. However, in some applications, involving aerial imaging for example or needing absolute measurement, another solution using solid state imaging and processing can be considered. Most of the time microlights fly in clear weather; observing the skyline by artificial vision can be considered as an option to solve the problem and to give an absolute attitude measurement. Electronic imagers are low-cost, reliable and light; fast electronic implementation is easy and a lot of off-the-shelf devices are available for real-time computing.

All of these considerations allow one to propose measurement systems based on electronic imagers (CCD, CMOS or a retinal imager) for the determination of attitude in clear weather. Imaging the horizon in such conditions gives a greyscale image that is almost sharp and highly contrasted with a bimodal histogram. The pixels from the ground are dark and those from the sky are lighter: binarization is made easier. Since this point is not the main concern of this paper, we will not develop it further. If necessary, a huge literature dealing with real-time image binarization is available and this issue can be easily addressed [2]. Some papers focus particularly on the horizon detection by artificial vision [6, 7]. The question of horizon detection has been studied extensively and robust solutions have been proposed. However, the emphasis is put on automatic piloting, basic flight stability and control of unmanned microlight aircraft and not on the metrological and algorithmic aspects of attitude determination [12], which are the issues addressed in this paper.

The attitude is characterized by two parameters: the rolling (rotation about the direction of flight) denoted θ and banking or pitch denoted φ (see figure 1). The yaw (ψ) is considered only as a noise input in our problem. Our devices are based on the following scheme: firstly a binarized skyline image is selected as a reference, then each shot, after binarization, is divided into two parts which mean values are subtracted to the corresponding data computed from the reference image. From this comparison analogue or digital values are deduced. This gives a way to estimate the roll and pitch variation angles.

The first system is made from off-the-shelf devices. The image is captured with a simple black and white CCD or CMOS camera, the resolution and acquisition rate of which

will define the precision and the rate of measurement. Very basic processing is performed by a dedicated electronic circuit that can be based on an FPGA (field-programmable gate array) circuit.

A second proposition for implementing our attitude estimation system is presented. It makes use of a CMOS retina dedicated to real-time, analogue intercorrelation computing. This ASIC (application specific integrated circuit), developed by our team (Laboratory for electronic and computer imaging of Le Creusot, France), delivers two signals proportional to the area of overlap between a current binarized image and a memorized one. It will be shown how this device can be useful for attitude measurement. Simple external processing implemented in a microcontroller completes the system.

The attitude control of airborne imaging systems and automatic pilot devices are the most obvious applications of this system [4, 13]. Because we don't use any sensor sensitive to gravitation or acceleration with respect to an absolute reference, the device that is proposed is very robust against vibrations and is not affected by gravitational variations.

A model for the proposed imaging system is presented in the next section. An equation for an ideal horizon image with respect to rolling and pitch angles is deduced in the following section. The method for estimating these angles from the image and the errors induced by the various approximations of the model are then proposed. In the next part a series of experimental results obtained from real images confirms the previous propositions. The last section is dedicated to a presentation of the retinal imager solution. Experimental results are also provided in this part. Finally some concluding remarks and propositions are given.

2. Camera modelling

The imager is supposed to be fixed on a gimballed platform that moves around the optical centre C. In a very classical approach a simple pinhole model is used for the camera. If the fixed coordinate system of the real world is denoted by Oxyz, the plane is assumed to be flying approximately straight along the Oz axis. The camera frame is CXYZ, where the optical axis is chosen as the CZ axis. The image reference plane (u, v), attached to the camera, is supposed to be perpendicular to the optical axis (see figure 1). Roll and pitch angles are denoted by θ (rotation about flying direction Oz) and φ (rotation about horizontal axis Oy); the yaw angle ψ (rotation about Ox) is assumed to be null.

The coordinates of point M are (xyz) in the fixed frame. Its coordinates in the camera coordinate system are (XYZ). They can be obtained (in homogeneous coordinate notation) with a rotation–translation matrix whose coefficients are the extrinsic parameters of the platform $[Rt]$:

$$[Rt] = \begin{bmatrix} r_{11} & r_{12} & r_{13} & t_x \\ r_{21} & r_{22} & r_{23} & t_y \\ r_{31} & r_{32} & r_{33} & t_z \\ 0 & 0 & 0 & 1 \end{bmatrix}. \tag{1}$$

R is a rotation matrix and is unitary ($R = R^{-T}$). A commonly used model for perspective cameras is that of linear projective mapping from 3D projective space to 2D projective space. This map is represented by a 3×4 matrix in homogeneous

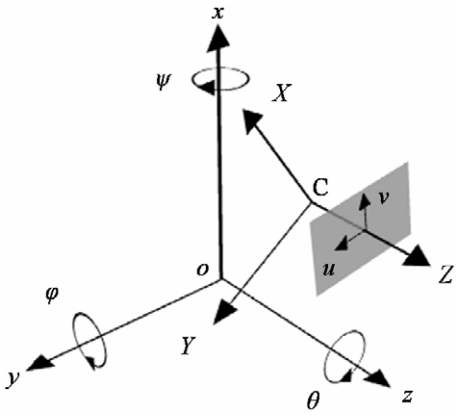

Figure 1. Camera on a gimballed platform.

coordinates. This point is projected onto the image plane in m of coordinates (u, v) measured in pixels in the image reference. The intrinsic parameters constitute the transformation matrix A,

$$A = \begin{bmatrix} \alpha & \gamma & u_0 & 0 \\ 0 & \beta & v_0 & 0 \\ 0 & 0 & 1 & 0 \end{bmatrix} \tag{2}$$

with (u_0, v_0) the coordinates of the principal point, α and β the scale factors in the image. The u and v axes measured in pixels (for instance, if focal length is 8 mm and pixels are squares of 10 μm width and height then $\alpha = \beta = 800$); γ is a parameter that describes the skewness of the two image axes [8].

Intrinsic parameters can be estimated in a classical calibration process [14]; self-calibration can be performed without the use of a calibration grid (see [9] for instance). As there are many other sources of error, the internal parameters given by the manufacturer are precise enough for this application. Therefore, s being an arbitrary scale factor, the coordinates of m with regard to those of M in the camera frame can be computed from

$$\begin{bmatrix} su \\ sv \\ s \end{bmatrix} = \begin{bmatrix} \alpha & \gamma & u_0 & 0 \\ 0 & \beta & v_0 & 0 \\ 0 & 0 & 1 & 0 \end{bmatrix} \begin{bmatrix} X \\ Y \\ Z \\ 1 \end{bmatrix}. \tag{3}$$

And the overall transform equation is

$$\begin{bmatrix} su \\ sv \\ s \end{bmatrix} = A[Rt] \begin{bmatrix} x \\ y \\ z \\ 1 \end{bmatrix}. \tag{4}$$

In the considered case, the extrinsic matrix is

$$[Rt] = \begin{bmatrix} \cos\theta\cos\varphi & \sin\theta\cos\varphi & -\sin\varphi & 0 \\ -\sin\theta & \cos\theta & 0 & 0 \\ \cos\theta\sin\varphi & \sin\theta\sin\varphi & \cos\varphi & t \\ 0 & 0 & 0 & 1 \end{bmatrix}. \tag{5}$$

3. Skyline modelling

3.1. Ideal skyline

The ideal skyline is the image of an ideal horizon, i.e. an infinite horizontal plane containing the origin which when

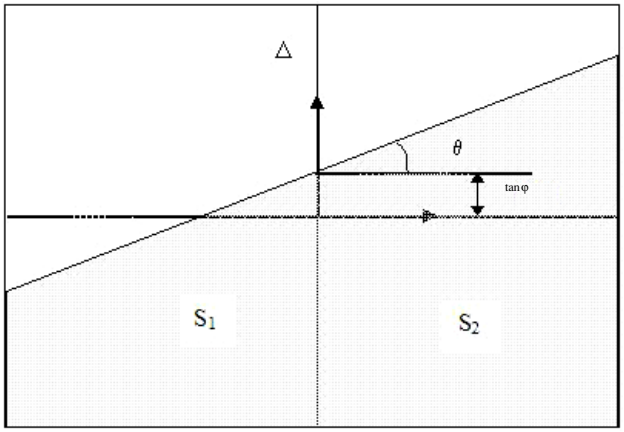

Figure 2. Ideal horizon image.

viewed in the object frame is a straight line parallel to the Oy axis:

$$x = 0, \qquad z = d. \tag{6}$$

As the real horizon is very far from the sensor, it is reasonable to consider that the translation factor t is negligible. In order to simplify the presentation and without any loss of generality the intrinsic model is supposed to be perfect: $u_0 = v_0 = \gamma = 0$. In these conditions, and forgetting the null last column, the overall transform matrix V is given by

$$V = \begin{bmatrix} \alpha\cos\theta\cos\varphi & \alpha\sin\theta\cos\varphi & -\alpha\sin\varphi \\ -\beta\sin\theta & \beta\cos\theta & 0 \\ \cos\theta\sin\varphi & \sin\theta\sin\varphi & \cos\varphi \end{bmatrix}; \tag{7}$$

therefore

$$\begin{bmatrix} su \\ sv \\ s \end{bmatrix} = V \begin{bmatrix} x \\ y \\ z \end{bmatrix}. \tag{8}$$

The skyline image is given by

$$\begin{cases} su = y\alpha\sin\theta\cos\varphi - d\alpha\sin\varphi \\ sv = y\beta\cos\theta \\ s = y\sin\theta\sin\varphi + d\cos\varphi. \end{cases} \tag{9}$$

Eliminating s and y leads to the skyline image equation

$$\frac{u}{\alpha} = \frac{v}{\beta}\frac{\tan\theta}{\cos\varphi} - \tan\varphi. \tag{10}$$

u and v are respectively the coordinates in line and column numbers counted from the middle of the sensor. In a normalized frame and for a small pitch, the coordinate of the crossing point between the skyline and the vertical axis is equal to the pitch angle φ and the angle between the skyline and the horizontal axis is approximately equal to the roll angle θ (figure 2). In practice, the measurable range of pitch angle is bounded by the sensor's dimensions and focal length. The skyline image line crosses the image borders at two points v_1 and v_2. The area on image of 'earth' region is given by (in an analogical approximation):

$$S = \frac{A}{2} + \int_{v_1}^{v_2} \left(v\frac{\alpha}{\beta}\frac{\tan\theta}{\cos\varphi} - \alpha\tan\varphi \right) \mathrm{d}v \tag{11}$$

A being the area of the sensor (the term $A/2$ has to be introduced because equation (10) is computed in the image-centred reference) and L its width in pixels.

3.2. Real skyline

Clearly the real-world skyline is not a straight line. This fact induces some discrepancies in the model when confronted with a real situation. The horizon can be modelled better by an injective function $x = h(y), z = d$ (d being very large in comparison with the focal length). As there are sometimes more than one value of x for each y the injective assumption is not verified if skyline is precisely considered. But, from a distant point of view such as that given by an airborne platform flying at an altitude of few tens of metres, the law of gravity and the forces of erosion that govern the progressive natural formation of terrain lighten the consequences of this constraint. In this model the skyline image is given by equation (8):

$$\begin{cases} su = x\alpha\cos\theta\cos\varphi + y\alpha\sin\theta\cos\varphi - d\alpha\sin\varphi \\ sv = -x\beta\sin\theta + y\beta\cos\theta \\ s = x\cos\theta\sin\varphi + y\sin\theta\sin\varphi + d\cos\varphi. \end{cases} \tag{12}$$

Eliminating the scale factor leads to the image skyline equation:

$$\frac{u}{\alpha} = \frac{-u\frac{\tan\varphi}{\alpha} + 1}{d} h\left(d\frac{u\frac{\sin\theta}{\alpha} + v\frac{\cos\theta}{\beta\cos\varphi} + \tan\varphi\sin\theta}{-u\frac{\tan\varphi}{\alpha} + 1} \right) + \frac{v}{\beta}\frac{\tan\theta}{\cos\varphi} - \tan\varphi. \tag{13}$$

The first term on the right-hand side of this equation can be seen as a correction to equation (10). If rotation angles are small (elementary rotations):

$$\frac{u}{\alpha} = \frac{1}{d} h\left(d\left(u\frac{\theta}{\alpha} + \frac{v}{\beta} + \varphi\theta \right) \right) + \frac{v}{\beta}\theta - \varphi. \tag{14}$$

If the skyline is plane enough, $u\frac{\theta}{\alpha}$ can be neglected in comparison with $\frac{v}{\beta}$. Neglecting also second order factors allows to simplify the equation:

$$\frac{u}{\alpha} \simeq \frac{1}{d} h\left(d\frac{v}{\beta} \right) + \frac{v}{\beta}\theta - \varphi. \tag{15}$$

The correction term is a dilated version of the horizon equation. The correction to the 'earth' area S (when considering only first order factors) does not depend on roll and pitch angles. We will show that our differential method, based on the movement of the skyline with respect to the angles, still matches even in real situations.

4. The influence of yaw movement

If the yaw movement (rotation of angle ψ around Ox) is taken into account, the extrinsic matrix become

$$[Rt] = \begin{bmatrix} \cos\theta\cos\varphi & \sin\theta\cos\varphi & -\sin\varphi & 0 \\ -\sin\theta\cos\psi + \cos\theta\sin\varphi\sin\psi & \cos\theta\cos\psi + \sin\theta\sin\varphi\sin\psi & \sin\psi\cos\varphi & 0 \\ \sin\theta\sin\psi + \cos\theta\sin\varphi\cos\psi & -\cos\theta\sin\psi + \sin\theta\sin\varphi\cos\psi & \cos\varphi\cos\psi & t \\ 0 & 0 & 0 & 1 \end{bmatrix}. \tag{16}$$

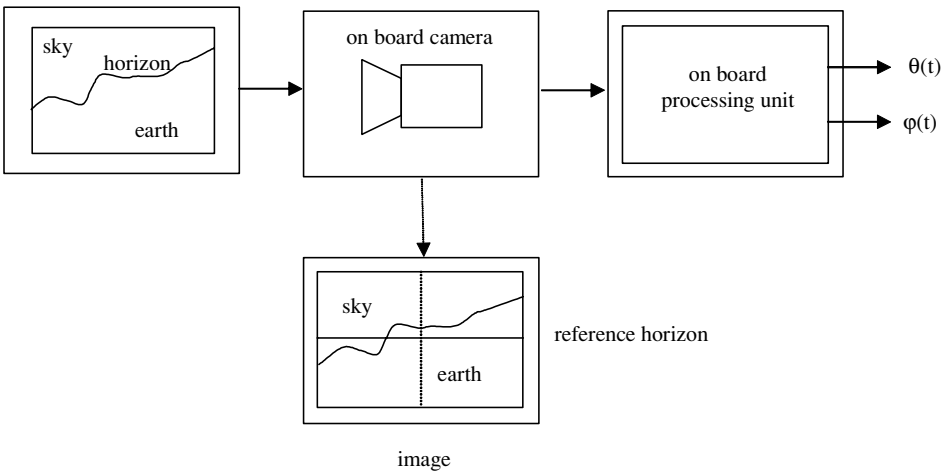

Figure 3. Description of the proposed device.

The ideal skyline image is given by

$$\begin{bmatrix} su \\ sv \\ s \end{bmatrix} = \begin{bmatrix} \alpha(\sin\theta\cos\varphi)y - \alpha(\sin\varphi)d \\ \beta(\cos\theta\cos\psi + \sin\theta\sin\varphi\sin\psi)y + \beta(\sin\psi\cos\varphi)d \\ (-\cos\theta\sin\psi + \sin\theta\sin\varphi\cos\psi)y + (\cos\varphi\cos\psi)d \end{bmatrix}. \tag{17}$$

The skyline equation in the image frame becomes

$$\frac{u}{\alpha} = \frac{v}{\beta}\left(\frac{\tan\theta\cos\psi}{\cos\varphi} - \tan\varphi\sin\psi\right) - \tan\varphi\cos\psi - \frac{\tan\theta\sin\psi}{\cos\varphi}. \tag{18}$$

In the approximation of small yaw angle and if the pitch is assumed to stay within limits, the only significant correction term $\psi\frac{\tan\theta}{\cos\varphi}$ is on the pitch value and it is proportional to the yaw angle. The determination of roll angle is hardly affected:

$$\frac{u}{\alpha} \simeq \frac{v}{\beta}\left(\frac{\tan\theta}{\cos\varphi}\right) - \tan\varphi - \psi\frac{\tan\theta}{\cos\varphi}. \tag{19}$$

5. A solution with an off-the-shelf camera

5.1. Absolute measurement

The proposed device is described in figure 3. The image is cut into two equal parts by a vertical axis Δ crossing through the centre of the image. The greyscale image is thresholded with regard to a reference value that can be defined either manually or automatically from a mean luminance value given for instance by an independent light sensor (a photodiode behind a diffusing glass). Other more sophisticated and robust segmentation methods for the skyline image can be found in [6, 7, 12]. Thresholding gives a binary image which pixels of value 0 correspond to the sky while those belonging to the 'earth', below the horizon, are set to 1. From this image, two parameters S_1 and S_2 are computed by counting pixel values from respectively the left and the right parts of this binary image (see figure 2). If only the simple case where the skyline crosses the two vertical image borders is considered, the S parameters are given by

$$S_1 = \frac{A}{4} + \int_{-\frac{L}{2}}^{0}\left(v\frac{\alpha}{\beta}\frac{\tan\theta}{\cos\varphi} - \alpha\tan\varphi\right)\mathrm{d}v \tag{20}$$

$$S_2 = \frac{A}{4} + \int_{0}^{\frac{L}{2}}\left(v\frac{\alpha}{\beta}\frac{\tan\theta}{\cos\varphi} - \alpha\tan\varphi\right)\mathrm{d}v. \tag{21}$$

Therefore the roll and pitch angles are determined by the equations

$$S_1 - S_2 = -\frac{L^2}{4}\frac{\alpha}{\beta}\frac{\tan\theta}{\cos\varphi} \qquad S_1 + S_2 = \frac{A}{2} - L\alpha\tan\varphi. \tag{22}$$

The pitch angle is given by the second equation; injecting it into the first equation leads to the determination of roll angle. If a first order approximation is considered, the computation is even simpler:

$$\theta \simeq \frac{4\beta}{L^2\alpha}(S_2 - S_1) \qquad \varphi \simeq \frac{\frac{A}{2} - (S_1 + S_2)}{L\alpha} \tag{23}$$

5.1.1. Measurement range. The measurement range of roll (in the linear zone) is limited by the angle between the image diagonal line and its horizontal axis; if l denotes the image height and if pitch is null:

$$|\tan\theta_{\max}| = \frac{\beta}{\alpha}\frac{l}{L}. \tag{24}$$

Pitch range is limited by image height; for roll equal to 0:

$$|\tan\varphi_{\max}| = \frac{l}{\alpha}. \tag{25}$$

5.1.2. Error linked to spatial image sampling. The image in a silicon electronic sensor is sampled, so the elementary image surface, i.e. the minimum measurement step, is the pixel size. The surfaces are measured up to ± 1 pixel. Therefore the angular resolution can be estimated from equations (23):

$$\Delta\theta \simeq \frac{8\beta}{L^2\alpha} \qquad \Delta\varphi \simeq \frac{2}{L\alpha}. \tag{26}$$

Confusing tangents and angles, the measurement minimum steps with regard to range are given by

$$\frac{\Delta\theta}{\theta_{\max}} \simeq \frac{8}{A} \qquad \frac{\Delta\varphi}{\varphi_{\max}} \simeq \frac{2}{A}. \tag{27}$$

In fact, with a classical camera, we will see that this cause of error is negligible in comparison with the others.

5.1.3. Error linked to approximation of the skyline model. As seen in section 3.2 the error due to the approximation of the real skyline by an ideal straight one does not depend on angles. It can be estimated from

$$\begin{aligned}\Delta S_1 &= \alpha \int_{-\frac{L}{2}}^{0} \frac{1}{d} h\left(d\frac{v}{\beta}\right) \mathrm{d}v = \frac{\alpha\beta}{d^2} \int_{-\frac{dL}{2\beta}}^{0} h(x)\,\mathrm{d}x \\ \Delta S_2 &= \alpha \int_{0}^{\frac{L}{2}} \frac{1}{d} h\left(d\frac{v}{\beta}\right) \mathrm{d}v = \frac{\alpha\beta}{d^2} \int_{0}^{\frac{dL}{2\beta}} h(x)\,\mathrm{d}x.\end{aligned} \tag{28}$$

Clearly, the horizon function has a majorant on the considered interval:

$$|h(x)| \leqslant H \quad \forall x \in \left[-\frac{dL}{2\beta}, \frac{dL}{2\beta}\right]; \tag{29}$$

therefore

$$|\Delta S_i| \leqslant \frac{\alpha L}{2d} H \tag{30}$$

and the error about the two parameters involved in the angle determination is bounded:

$$|\Delta(S_0 + S_1)| = |\Delta(S_0 - S_1)| \leqslant \frac{\alpha L}{d} H. \tag{31}$$

The relative error on angles is approximately equal to $\frac{H}{d}$; in mountainous country it can be quite noticeable but it can be supposed to stay below 10% in normal conditions, i.e. a skyline distance of several kilometres and a landscape with hills no higher than a few hundred metres. Further it will be shown that this error can be avoided when only a differential determination is desired.

5.1.4. Error due to yaw movement. We have seen that if the yaw movement is not negligible the equation for the skyline image is given by

$$\begin{aligned}\frac{u}{\alpha} = \frac{v}{\beta}\left(\frac{\tan\theta\cos\psi}{\cos\varphi} - \tan\varphi\sin\psi\right) \\ - \tan\varphi\cos\psi - \frac{\tan\theta\sin\psi}{\cos\varphi}.\end{aligned} \tag{32}$$

Therefore

$$\begin{aligned}S_1 - S_2 &= -\frac{L^2}{4}\frac{\alpha}{\beta}\left(\frac{\tan\theta\cos\psi}{\cos\varphi} - \tan\varphi\sin\psi\right) \\ S_1 + S_2 &= \frac{A}{2} - L\alpha\left(\tan\varphi\cos\psi + \frac{\tan\theta\sin\psi}{\cos\varphi}\right).\end{aligned} \tag{33}$$

In a small-angle approximation:

$$\begin{aligned}S_1 - S_2 &= -\frac{L^2}{4}\frac{\alpha}{\beta}\left(\frac{\tan\theta}{\cos\varphi} - \psi\tan\varphi\right) \\ S_1 + S_2 &= \frac{A}{2} - L\alpha\left(\tan\varphi + \psi\frac{\tan\theta}{\cos\varphi}\right).\end{aligned} \tag{34}$$

If the pitch stays within limits, its determination is the only one concerned, especially if the rolling is noticeable:

$$S_1 + S_2 \simeq \frac{A}{2} - L\alpha(\tan\varphi + \psi\tan\theta). \tag{35}$$

Unfortunately, this error will be still present in the differential mode presented in the next part.

5.2. Differential measurement

On the one hand, in most applications such as attitude control or gimballed platform control, only a measure of the variation of attitude is needed. On the other hand, generally speaking, a differential approach allows the effect of some error sources to be limited. These considerations lead us toward a proposition for a method for differential measurement of attitude. Two stages are involved. In the first one, reference horizon parameters are recorded. For that an image is shot and the reference parameters called S_{10} and S_{20} representing the luminance of the left and right parts of the binarized image respectively are stored. In the second stage, current images are shot at a given rate. Each of them is binarized (the threshold can be updated if necessary with regard to current illumination conditions) and yields the current parameters S_1 and S_2. These current parameters are compared with the reference ones. The angle variations between the current image and the reference one can be deduced:

$$\begin{aligned}\frac{\tan\theta_1}{\cos\varphi_1} - \frac{\tan\theta_0}{\cos\varphi_0} &= -\frac{4\beta}{L^2\alpha}[(S_1 - S_2) - (S_{10} - S_{20})] \\ \tan\varphi_1 - \tan\varphi_0 &= -\frac{(S_1 + S_2) - (S_{10} + S_{20})}{L\alpha}.\end{aligned} \tag{36}$$

If angle variations are small:

$$\begin{aligned}\tan\varphi_1 &\simeq \tan\varphi_0 + \frac{1}{\cos^2\varphi_0}(\varphi_1 - \varphi_0) \\ \frac{\tan\theta_1}{\cos\varphi_1} &\simeq \frac{\tan\theta_0}{\cos\varphi_1} + \frac{1}{\cos\varphi_1\cos^2\theta_0}(\theta_1 - \theta_0).\end{aligned} \tag{37}$$

In a first order approximation, the roll angle $\Delta\theta = \theta_0 - \theta_1$ and pitch angle $\Delta\varphi = \varphi_0 - \varphi_1$ with regard to the reference horizon are given by

$$\begin{aligned}\Delta\theta &= \frac{4\beta}{L^2\alpha}[(S_1 - S_2) - (S_{10} - S_{20})] \\ \Delta\varphi &= \frac{(S_1 + S_2) - (S_{10} + S_{20})}{L\alpha}.\end{aligned} \tag{38}$$

If the equation of the skyline does not change during the shoot, the error linked to the real skyline approximation disappears (in a first order computation). The part of the error introduced by a small-angle approximation can be avoided by inserting an approximate value for the roll angle (obtained by the direct algorithm described in the previous section).

Our method to determine the roll and pitch angles is efficient and fast. The electronic implementation is easy, and the camera line and frame-synchronized counters are the only hardware required to obtain S_1 and S_2. Even the subtracters and adders can be avoided by astutely presetting the counters with stored reference values S_{10} and S_{20}. Very simple hardware allows determination of attitude angles at a standard video scan rate of 25 or 30 frames s^{-1}. Our artificial vision device for the relative attitude measurement of an airborne platform is a real-time one and it fits well the control application requirements.

5.3. Experimental results

Some experiments have been performed outdoors in order to illustrate the feasibility and estimate the precision obtained in a real situation. An experimental demonstration was not really intended. Simple and contrasting landscapes were chosen.

Figure 4. Example of a real horizon.

The shooting device is a simple low-cost still camera that stands on a stable calibrated steerable support allowing angle measurements. Figure 4 shows an example of an image of the horizon shot during these experiments. As our aim was just to illustrate the feasibility, we chose to use as intrinsic parameters of the camera the ones given in the constructor's data sheet:

$$L = 1280, \quad l = 960, \quad \alpha = \beta = 4350. \tag{39}$$

Yet in an operational implementation a real calibration process has to be performed to obtain the best results. The measurement range is computed from equations (24) and (25):

$$\theta_{\max} = \pm 36.9^\circ \qquad \varphi_{\max} = \pm 6.23^\circ. \tag{40}$$

The theoretical error due to spatial sampling is less than $3 \times 10^{-4\circ}$. For $d \geqslant 2000$ m and $H \leqslant 20$ m, the relative error due to the real horizon equation can be bounded by 1% for these experiments.

The results are illustrated in figure 5. Curves (*a*) and (*b*) of figure 5 summarize about 20 experimental points for the roll and pitch obtained with various types of landscapes, various yaw angles (within a $\pm 15^\circ$ range) and various attitudes. The best straight line in the least square sense is computed, its slope is 0.97 and the standard deviation is about 0.49° for the roll, while it is a little bit better for the pitch with a slope equal to 0.98 and standard deviation of 0.40°. Since a perfect result should be 1 for the slopes, the residual systematic error is less than 2 or 3%. One can consider that the theoretical predictions about errors due to spatial sampling and skyline approximation are verified for the experimental conditions involved. Curve (*c*) of figure 5 is typical of the experimental dependence of roll on yaw in a real situation. The pitch range is so tight that no systematic influence of yaw has been experimentally assessed. Further experiments with a smaller focal length should be conducted to verify the theoretical prediction about the influence of yaw.

6. Solution with CMOS retina

Thanks to the development of CMOS technology it is now easy to implement an image sensor and its dedicated processing unit on the same chip. Bio-inspired retinal circuit [3], hardware implementation of classical image processing algorithm [10] or all-purpose reprogrammable device [5], it does not matter. The main point is to be able to process the data in the most parallel way and therefore to transmit only the pertinent information, avoiding the bottleneck of serial image transmission from the sensor to the processing unit. Such a device has been designed and realized in our lab [1]. Its

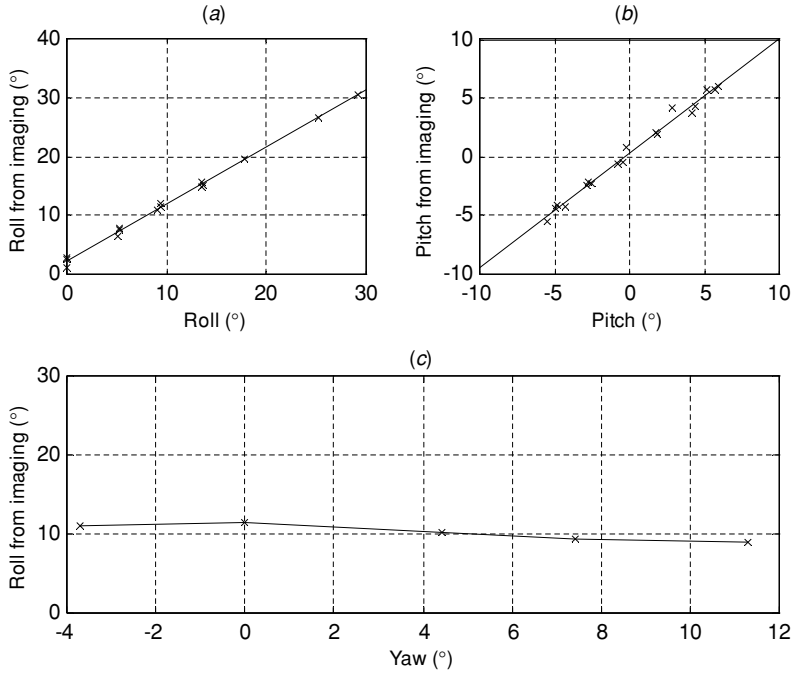

Figure 5. Experimental results. (*a*) Roll from imaging versus direct measurement with the best straight line fits. (*b*) Pitch from imaging versus direct measurement with the best straight line fits. (*c*) Roll versus yaw (angles in degrees).

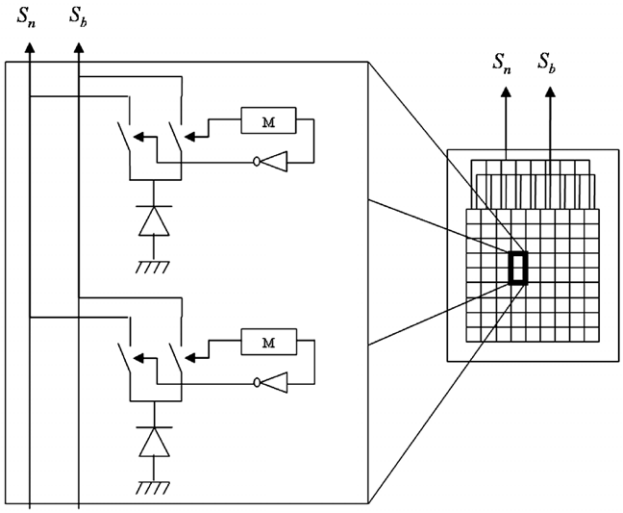

Figure 6. Schematic view of the circuit.

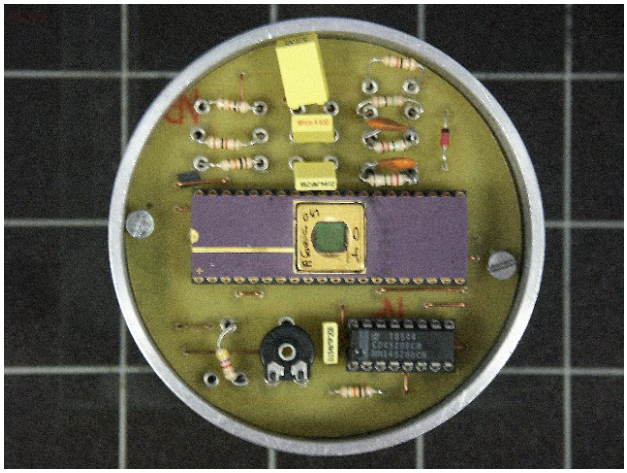

Figure 7. Retinal device (background squares are 2.54 × 2.54 cm).

original purpose is to recognize and to follow a moving object in real-time applications. But it appears that it can be useful for attitude measurement and control. As airborne devices are under consideration, the weight, size and power consumption are of prime importance. The CMOS retinal solution leads to an improvement on these points with respect to one based on the now classical 'smart cameras' embedding on-board DSP capability. This point is shown in table 1, which gives the typical main specifications of these devices.

Table 1. Specifications of the 'smart camera' and CMOS retinal solution.

	'Smart camera'	CMOS retinal
Resolution (pixels)	640 × 480	100 × 100
Power	5 W	60 mW
Mass (without lens)	170 g	50 g
Size (mm)	110 × 60 × 30	75 × 50 × 10

6.1. Circuit presentation

A highly simplified view of the circuit structure is presented in figure 6. The light-sensitive part for each pixel is a photodiode whose output ($Ilum(x, y)$, a current proportional to the light flux) is driven to either S_b or S_n. The choice is defined by the value of a binary memorized mask $M(x, y)$.

$$S_b = k \sum_x \sum_y M(x, y) Ilum(x, y)$$

$$S_n = k \sum_x \sum_y \overline{M}(x, y) Ilum(x, y).$$

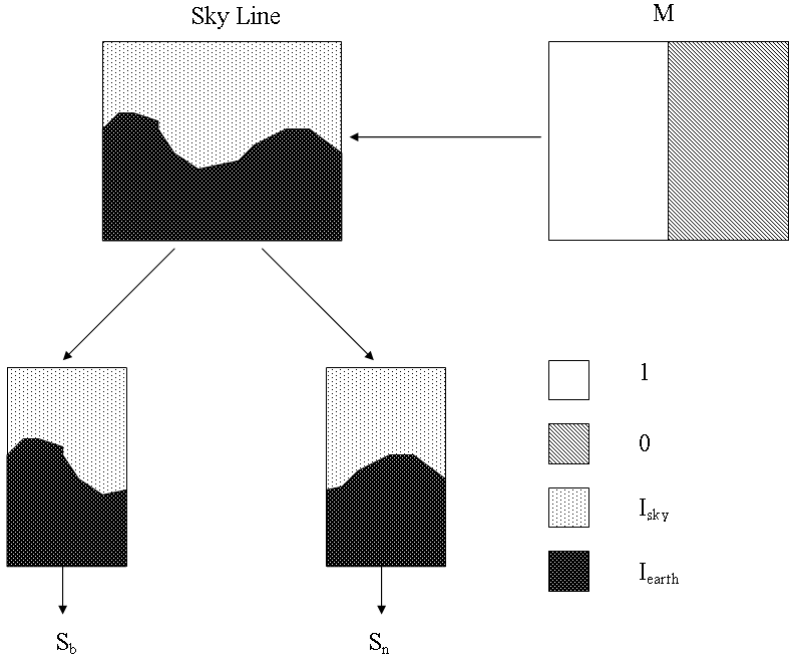

Figure 8. Masking and shooting with the retinal circuit.

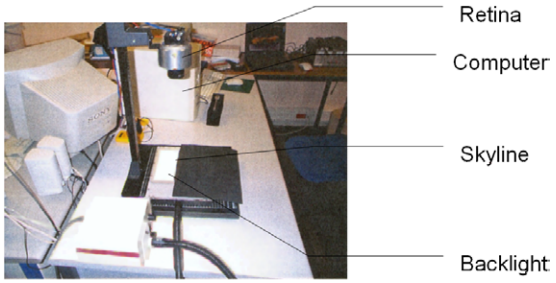

Figure 9. View of the experimental set-up for the retinal circuit.

$\overline{M}$ is defined by $\overline{M} = 1 - M$ and k is a sensor parameter. Two resistor backfed operational amplifiers convert current outputs into voltage ones. The mask M is memorized off-line; in this training stage an image is optically projected onto the sensor and the result is binarized. Following this scheme a 100×100 pixels CMOS retinal circuit has been realized in the 0.6 μm technology of Austria Microsystem (figure 7). It should be noted that even with such a low spatial resolution the error in angle estimate due to spatial sampling stays within acceptable limits (namely under 10^{-4}).

6.2. Application to attitude measurement and control

For application to attitude measurement, the mask is a binary image in which the surface is divided into two homogeneous parts of equal surface area by a vertical straight line (figure 8). With this configuration, the outputs are given by

$$\begin{aligned} S_b &= \frac{kI_+A}{2} - k(I_+ - I_-)S_1 \\ S_n &= \frac{kI_+A}{2} - k(I_+ - I_-)S_2. \end{aligned} \tag{41}$$

A is still the sensor surface; S_1 and S_2 are the parameters already defined. I_+ and I_- are the output currents for a pixel from the sky and from the earth. From these outputs, knowing the system constants, $S_1 + S_2$ and $S_1 - S_2$ are easily deduced and thus roll and pitch angles can be obtained.

6.3. Experimental results

In order to verify the ability of our retinal circuit to measure attitude angles, a laboratory experiment has been conducted. The experimental set-up can be seen in figure 9. An artificial horizon has been simulated with a sheet of black paper placed in front of a backlight. Pitch and roll are mimicked by moving the black sheet. Pitch variations are simulated by vertically translating the black sheet while roll is obtained by simply rotating the sheet. S_b and S_n are digitalized and input into a computer to give angle values. During a preliminary calibration phase, the system constants ($kI_\pm$) are determined. Two measurements have to be performed: in the first one (a), the black sheet is disposed so that the camera field of view is covered with a sky-only landscape ($S_1 = S_2 = 0$):

$$(a) \quad kAI_+ = S_b + S_n. \tag{42}$$

In the second step (b), an all-earth view is shot $\left(S_1 = S_2 = \frac{A}{2}\right)$:

$$(b) \quad kAI_- = S_b + S_n. \tag{43}$$

It is clear that this calibration phase can be easily performed in a real situation by aiming the camera first at the sky and then at the earth. As previously pointed out, pitch variations lead to vertical translations ($\Delta\varphi$) of the horizon while rolling is seen as a rotation ($\Delta\theta$) of this line. Those movements are deduced from the output S_b and S_n. Experimental results are summarized in figure 10. This shows that roll and pitch angles are in a quasilinear dependence on S_b and S_n and that roll and pitch influences are decorrelated. For example, let us consider the evolution of the output signals of the retina for seven values of roll and pitch corresponding to points P1 to P7 in figure 10. One pair of values (S_b, S_n) corresponds

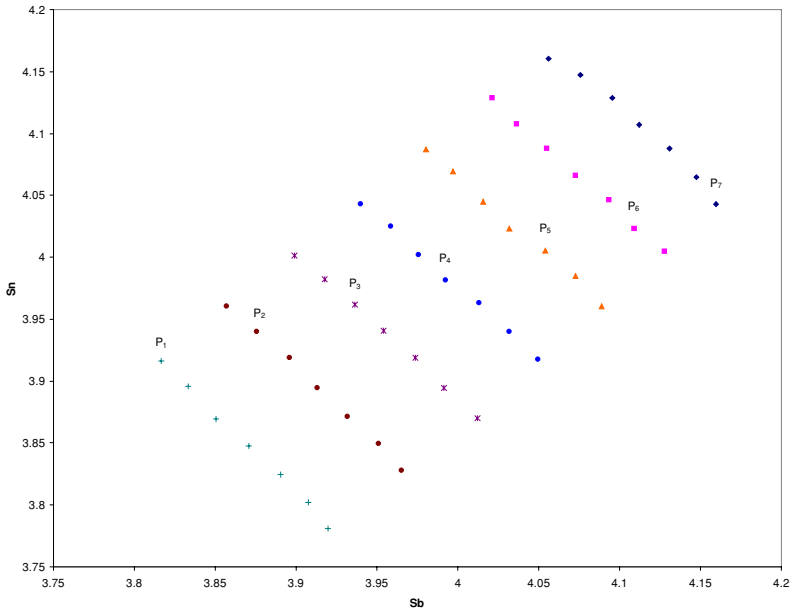

Figure 10. Experimental results: values of (S_b, S_n) for linear variations of the pitch and roll. One pair of values (S_b, S_n) corresponds to only one pair of values (φ, θ).

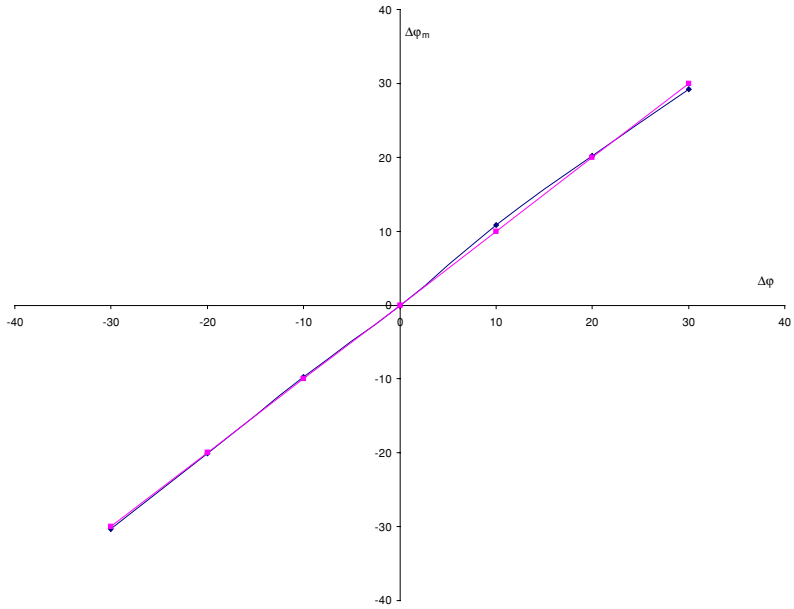

Figure 11. Pitch deduced from S_b, S_n with respect to the theoretical value.

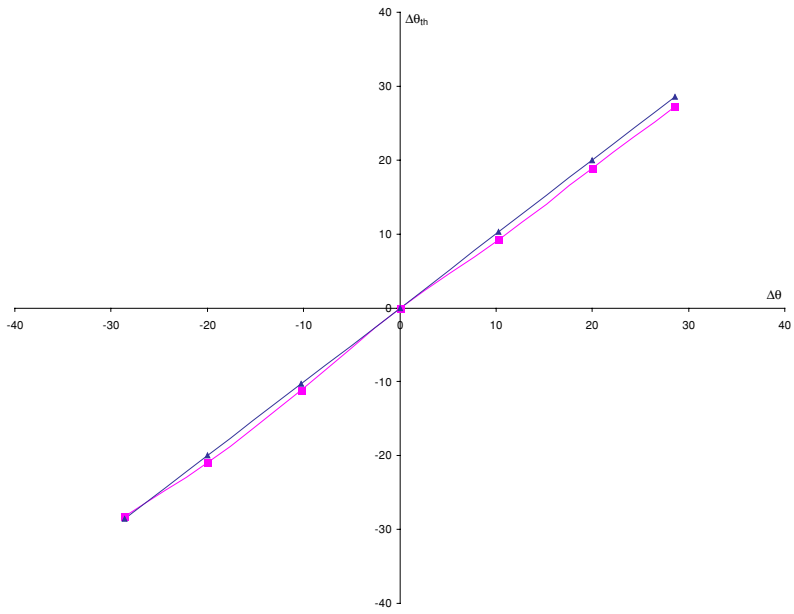

Figure 12. Roll deduced from S_b, S_n with respect to the theoretical value.

to only one pair of values (θ, φ). Then, using equations presented in sections 3.1 and 3.2, it is possible to determine a measured relative value (denoted $(\Delta\theta_m, \Delta\varphi_m)$) of (θ, φ). In figure 11 the 'square' curve presents the relationship between $\Delta\varphi_m$ and $\Delta\varphi$. Compared with the ideal relationship presented by the 'triangle' curve, the relative absolute error is less than 2.46%. For $\Delta\theta_m$ and $\Delta\theta$, in figure 12, the relative error is less than 5%.

The purpose of the experimental sections is only to illustrate the feasibility of the proposed devices; a more precise and complete study of the experimental precision in real situation should be conducted. But it would need a precise application context to be really conclusive.

7. Conclusion

A theoretical study of the conditions for measuring attitude angles from artificial vision has been proposed and an original practical algorithm allowing these measurements to be performed in real time has been described. An implementation in a CMOS retinal circuit is also presented. These points are illustrated by some experiments confirming the feasibility of the device. Some questions are still to be studied. If this sensor is to be used under bad lighting conditions, or particular skyline features, the implementation of a robust, real time, horizon detection algorithm has to be proposed. For a given application, precise experiments have

to be done to estimate the precision of the pitch and roll measurements.

Some other ideas for improvements or extensions deserve thorough study. For instance, it appears that reliability could be increased by diversity. Indeed, if a plate beamsplitter associated with two complementary colour filters is placed behind the objective of a colour CCD camera, keeping one image from each colour channel, two images of the skyline from two sides of the flying vector can be obtained. Two independent measurements can be performed simultaneously to provide an exploitable result even in bad conditions—sun in front, horizon partly fogged etc. Each point of view gives a complementary observation to the other; roll corresponds to pitch and vice versa. Therefore, errors affecting specifically one of these two quantities (pitch error when yaw is noticeable) can be eliminated. Finally the precision can easily be improved by taking into account a value of yaw angle given by a simple magnetic compass.

References

[1] Aubreton O, Bellach B, Lew Yan Voon L F C, Lamalle B, Gorria P and Cathebras G 2004 Retina for pattern matching in standard 0.6 μm CMOS technology *J. Electron. Imaging* **13** 559–69

[2] Castleman K R 1996 *Digital Image Processing* (Englewood Cliffs, NJ: Prentice-Hall)

[3] Curuciello E, Cumings R E and Boahen K A 2003 A biomorphic digital image sensor *IEEE J. Solid State Circuit* **38** 281–94

[4] Devaux J C, Gouton P and Truchetet F 2001 The Karhunen–Loeve transform applied to region-based segmentation of color aerial images *Opt. Eng.* **40** 1302–8

[5] Dudeck P and Hicks P J 2001 An SIMD focal plane analogue processor array *ISCAS'2001 (May)*

[6] Ettinger S M, Nechyba M C, Ifju P G and Waszak M 2002 Towards flight autonomy: vision-based horizon detection for micro air vehicles *Proc. Florida Conf. on Recent Advances in Robotics, FCRAR 2002 (Miami, May)*

[7] Ettinger S M, Nechyba M C, Ifju P G and Waszak M 2003 Vision-guided flight stability and control for micro air vehicles *Adv. Robot.* **17** 617–40

[8] Faugeras O D 1993 *Three-Dimensional Computer Vision: a Geometric Viewpoint* (Cambridge, MA: MIT Press)

[9] Hartley R I 1994 An algorithm for self calibration from several views *Proc. IEEE Conf. on Computer Vision and Pattern Recognition (Seattle, June)* pp 908–12

[10] Navaro D, Cathebras G and Gensolen F 2003 A block matching approach for movement estimation in a CMOS retina: principle and results *IEEE ESSIRC'03: 29th European Solid State Circuits Conference (Lisbon, Portugal, September)*

[11] Sullivan D and Brown A 2002 High accuracy autonomous image georeferencing using a GPS/Inertial-aided digital imaging system *Proc. of ION National Technical Meeting 2002 (San Diego, January)*

[12] Todorovic S and Nechyba M C 2004 A vision system for intelligent mission profiles of micro air vehicles *IEEE Trans. Veh. Technol.* **53** 1713–25

[13] Vioix J B, Douzals J P, Truchetet F, Guillemin J P and Assemat L 2002 Spatial and spectral methods for weed detection and localization *Eurasip J. Appl. Signal Process.* **7** 679–85

[14] Zhang Z 1998 A flexible new technique for camera calibration *Tech. Report* MSR-TR-98-71 Microsoft Research http://research.microsoft.com/~zhang